Monthly Notices of the ROYAL ASTRONOMICAL SOCIETY
MNRAS **502,** 4972–4980 (2021)
Advance Access publication 2021 February 15
doi:10.1093/mnras/stab439

Hidden in plain sight: a double-lined white dwarf binary 26 pc away and a distant cousin

Mukremin Kilic[1]★ A. Bédard[2] and P. Bergeron[2]
[1]Homer L. Dodge Department of Physics and Astronomy, University of Oklahoma, 440 W. Brooks St., Norman, OK 73019, USA
[2]Département de Physique, Université de Montréal, C.P. 6128, Succ. Centre-Ville, Montréal, QC H3C 3J7, Canada

Accepted 2021 February 5. Received 2021 February 4; in original form 2020 December 10

ABSTRACT
We present high-resolution spectroscopy of two nearby white dwarfs with inconsistent spectroscopic and parallax distances. The first one, PG 1632+177, is a 13th magnitude white dwarf only 25.6 pc away. Previous spectroscopic observations failed to detect any radial velocity changes in this star. Here, we show that PG 1632+177 is a 2.05-d period double-lined spectroscopic binary (SB2) containing a low-mass He-core white dwarf with a more-massive, likely CO-core white dwarf companion. After L 870−2, PG 1632+177 becomes the second closest SB2 white dwarf currently known. Our second target, WD 1534+503, is also an SB2 system with an orbital period of 0.71 d. For each system, we constrain the atmospheric parameters of both components through a composite model-atmosphere analysis. We also present a new set of non-local thermodynamic equilibrium (NLTE) synthetic spectra appropriate for modelling high-resolution observations of cool white dwarfs, and show that NLTE effects in the core of the H α line increase with decreasing effective temperature. We discuss the orbital period and mass distribution of SB2 and eclipsing double white dwarfs with orbital constraints, and demonstrate that the observed population is consistent with the predicted period distribution from the binary population synthesis models. The latter predict more massive CO + CO white dwarf binaries at short (<1 d) periods, as well as binaries with several day orbital periods; such systems are still waiting to be discovered in large numbers.

Key words: stars: evolution – stars: individual: WD 1534+503 (GD 347) – stars: individual: PG 1632+177 – white dwarfs.

1 INTRODUCTION

Double-lined spectroscopic binaries (SB2) are the best: Radial velocity measurements of both stars in the system enable a direct measurement of the gravitational redshifts, masses, the mass ratio, and the inclination of the binary. However, double-lined binaries are hard to identify in low-resolution spectroscopy that is typical in large-scale surveys like the Sloan Digital Sky Survey. This is one of the challenges that prevents us from detecting the double white dwarf progenitors of type Ia supernovae (Rebassa-Mansergas et al. 2019).

Population synthesis models indicate that double white dwarfs should be relatively common in the Galaxy, and they dominate the gravitational wave foreground in the milli-Hertz frequency range (Nissanke et al. 2012; Korol et al. 2017). Radial velocity surveys targeting low-mass white dwarfs (Marsh, Dhillon & Duck 1995; Kilic et al. 2010; Brown et al. 2010, 2020) and high-cadence, wide-field photometric surveys (Burdge et al. 2019a,b, 2020) have been successful in finding short-period double white dwarfs. However, low-mass white dwarfs typically outshine their companions, and SB2 systems have been elusive. Saffer, Liebert & Olszewski (1988) identified L 870−2 as the first SB2 white dwarf binary with a period of 1.6 d. However, in the following three decades, only about two dozen additional systems have been identified (Napiwotzki et al. 2020).

Trigonometric parallax measurements provide an opportunity to find SB2 white dwarfs through their overluminosity. Bédard, Bergeron & Fontaine (2017) used a sample of 219 white dwarfs with parallax measurements to identify more than a dozen overluminous white dwarfs, and Kilic et al. (2020) confirmed binarity in at least nine out of 13 of these systems, including four SB2 white dwarfs. Similarly, Hollands et al. (2018) analysed the nearly complete *Gaia* 20 pc white dwarf sample of 139 stars, and identified several overluminous binary candidates, including L 870−2.

Here we present high-resolution spectroscopy of two new SB2 white dwarfs, WD 1534+503 and PG 1632+177, and constrain their orbits. We describe the details of our target selection and observations in Sections 2 and 3, and present the radial velocity measurements, orbital, and physical parameters of these binary systems in Sections 4, 5, and 6, respectively. We present a new set of non-local thermodynamic equilibrium (NLTE) synthetic spectra for cool white dwarfs along with a comparison with the observed line profiles in WD 1534+503 and PG 1632+177 in Section 7. We discuss the properties of the current population of SB2 white dwarfs in Section 8, and conclude.

2 TARGET SELECTION

We selected WD 1534+503 and PG 1632+177 for follow-up observations due to the inconsistencies between their spectroscopic distance and parallax. Using the spectroscopic method, Gianninas, Bergeron & Ruiz (2011) derived $T_{\rm eff}$ = 9010 ± 130 K, $\log g$ = 8.14 ± 0.05 for WD 1534+503 based on 1D model atmospheres (see also Tremblay, Bergeron & Gianninas 2011; Kleinman et al.

★ E-mail: kilic@ou.edu

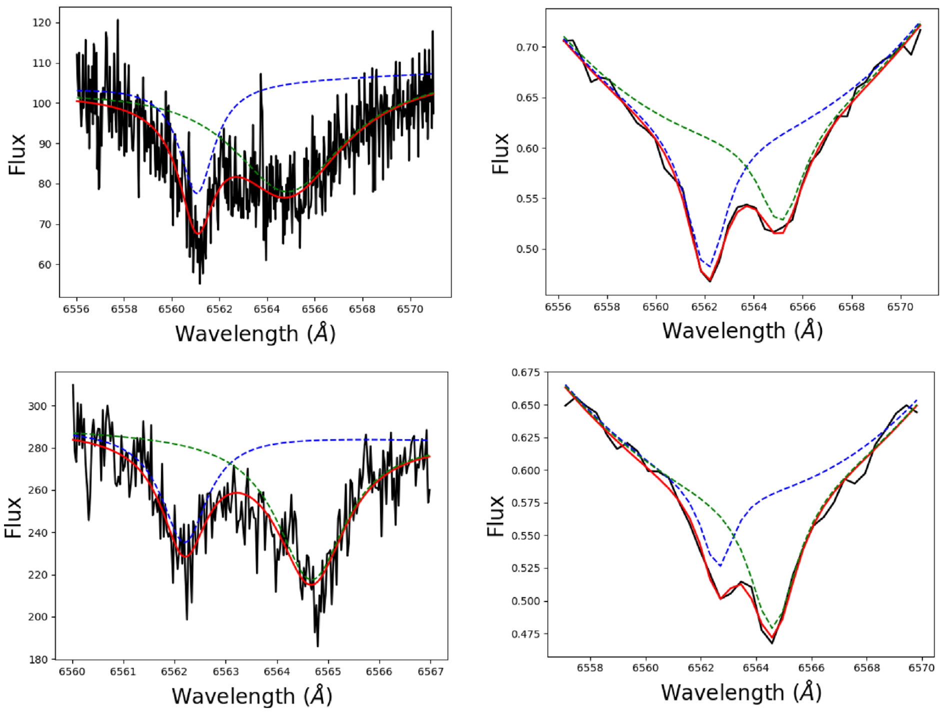

Figure 1. Best-fitting Lorentzian profiles (blue and green dotted lines) to the H α line cores visible in the Keck (left-hand panels) and Gemini (right-hand panels) spectra of WD 1534+503 (top panels) and PG 1632+177 (bottom panels). The red solid lines show the composite best-fitting Lorentzian profiles.

2013). Including the 3D corrections from Tremblay et al. (2013), the best-fitting parameters are $T_{\rm eff}$ = 8960 K, log g = 7.87, and a spectroscopic distance of 45.1 pc. However, *Gaia* Data Release 2 parallax (Gaia Collaboration et al. 2018) puts WD 1534+503 at 68.5 pc. Hence, it is significantly brighter than expected for a single white dwarf. Interestingly, Zuckerman et al. (2003) obtained a high-resolution spectrum of WD 1534+503 to search for metal lines, and they noted the detection of two H β components in this system, and labelled it as a 'possible newly identified double degenerate' in their table 2. No further follow-up has been done since then.

Similarly, Gianninas et al. (2011) used the spectroscopic method to derive $T_{\rm eff}$ = 10, 220 ± 150 K, log g = 8.04 ± 0.04 for PG 1632+177. Including the 3D corrections from Tremblay et al. (2013), the best-fitting parameters are $T_{\rm eff}$ = 10, 020 K, log g = 7.80, and a spectroscopic distance of 17.1 pc. However, *Gaia* DR2 parallax puts PG 1632+177 at a distance of 25.6 pc, again indicating that this is also an overluminous white dwarf. Interestingly, Saffer, Livio & Yungelson (1998) searched for radial velocity variations in PG 1632+177, but did not find any significant variations. However, their spectral resolution of 3 Å and their observing cadence of two observations separated by 1–2 h on a single night, followed by a third observation 1 or 2 d later likely made it impossible to detect the double-lines in this ≈2 d (see below) orbital period system.

3 OBSERVATIONS

We used the HIRES echelle spectrometer (Vogt et al. 1994) on the Keck I telescope to observe our two targets on UT 2018 June 18. Due to volcanic activity, our observations were limited to a period of only 2 h, over which we were able to get a single spectrum of WD 1534+503, and four spectra of PG 1632+177. We used the blue cross disperser with a 1.15-arcsec slit resulting in a spectral resolution of 37 000. We used MAKEE to analyse the HIRES data, and detected double H α lines for both objects.

We obtained follow-up optical spectroscopy of both targets using the 8-m Gemini telescope equipped with the Gemini Multi-Object Spectrograph (GMOS) as part of the queue program GN-2020A-Q-221. We used the R831 grating and a 0.25-arcsec slit, providing wavelength coverage from 4585 to 6930 Å and a resolution of 0.98 Å. Each spectrum has a comparison lamp exposure taken within 10 min of the observation time. We used the IRAF GMOS package to reduce these data.

Our initial observing strategy at Gemini was to obtain two to three spectra over 4–5 h on a single night, and repeat this sequence on additional nights as the queue schedule permitted. This worked well for WD 1534+503. However, we realized after the initial observations on PG 1632+177 that its orbital period is much longer than 4–5 h, and we changed our observing cadence to a single observation per night for the last four epochs.

4 RADIAL VELOCITY MEASUREMENTS

We use the same procedures as in Kilic et al. (2020) to measure radial velocities for our targets. Briefly, we use a quadratic polynomial plus two Lorentzians (one for each line) to fit the H α line cores. We use LMFIT, a version of the Levenberg–Marquardt algorithm adapted for PYTHON (Newville et al. 2014), to find the best-fitting parameters. We apply the standard Solar system barycentric corrections, and use the night skylines to correct for the spectrograph flexure.

Fig. 1 shows the Keck (left-hand panels) and Gemini (right-hand panels) spectra of WD 1534+503 (top panels) and PG 1632+177 (bottom panels) along with the best-fitting Lorentzian profiles to the H α line cores. The red line shows the best-fitting composite profiles in each case. Here we show Gemini spectra at a similar orbital phase to the Keck spectra so that a fair comparison can be made. Luckily,

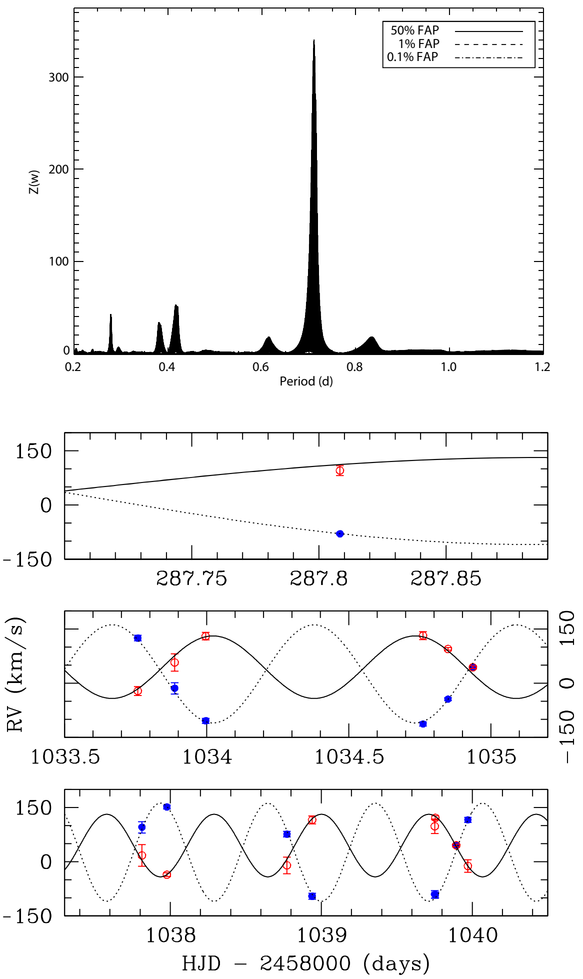

Figure 2. Top panel: Lomb–Scargle periodogram for WD 1534+503. Middle and bottom panels: radial velocity measurements (open and filled points) of the two components of the WD 1534+503 system. The solid and dotted lines show the best-fitting orbit for each component, assuming a circular orbit.

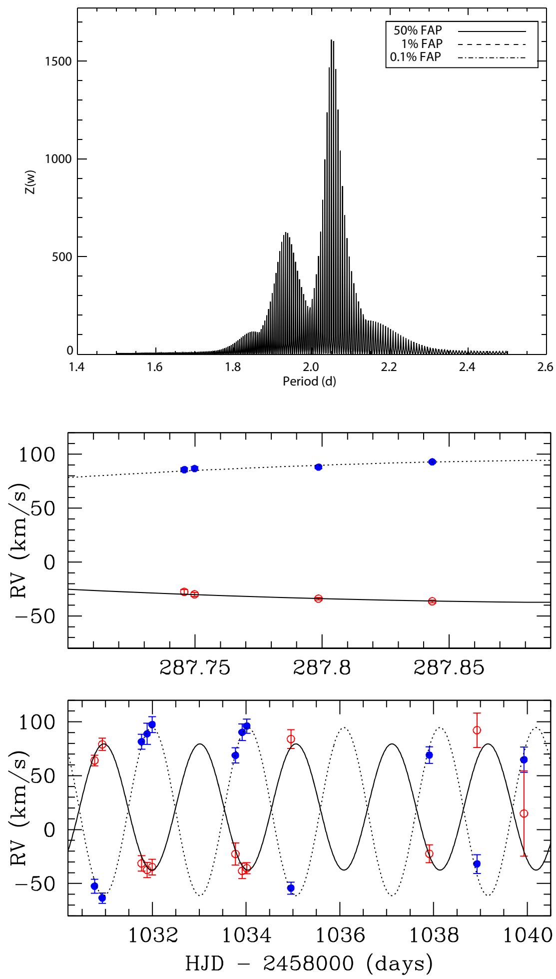

Figure 3. Top panel: Lomb–Scargle periodogram for PG 1632+177. Middle and bottom panels: radial velocity measurements (open and filled points) of the two components of the PG 1632+177 system. The solid and dotted lines show the best-fitting orbit for each component, assuming a circular orbit.

for both WD 1534+503 and PG 1632+177, one of the H α line cores is significantly deeper than the other, enabling us to reliably identify the lines at different orbital phases.

We use bootstrapping to estimate the errors in radial velocities as formal fitting errors tend to be underestimated (Napiwotzki et al. 2020). We randomly select N points of the observed spectra, where points can be selected more than once, to rederive velocities, repeating this procedure 1000 times. Tables A1 and A2 present our radial velocity measurements for WD 1534+503 and PG 1632+177, respectively. In two of the epochs, we caught WD 1534+503 near conjunction, with only a single H α line visible in the system. These measurements are included in Table A1, but not used in the orbital fits as it is impossible to measure the centres for both lines accurately. Similarly, the lines are significantly blended in our last spectrum of PG 1632+177, and these measurements are included in Table A2, but not used in the orbital fits.

5 ORBITAL PARAMETERS

Fig. 2 shows the radial velocity measurements and the Lomb–Scargle periodogram for WD 1534+503. The period is relatively well constrained to 0.71 d in this system. We use the IDL program MPRVFIT (De Lee et al. 2013) in the SB2 mode to find the best-fitting orbit. Excluding the spectra where the H α lines from both stars overlap and appear as a single line, we have 13 radial velocity measurements. The solid and dotted lines show the best-fitting orbital solution for each star.

Period aliases are the largest source of uncertainty in the orbital fits. We use a Monte Carlo approach, re-sampling the radial velocities with their errors and re-fitting orbital parameters 1000 times. We report the median value and errors derived from the 15.9 and 84.1 per cent percentiles of the distributions for each orbital element. The best-fitting orbital parameters are $P = 0.711\,29^{+0.002\,86}_{-0.001\,35}$ d, $K_1 = 135.9^{+3.3}_{-3.1}$ km s^{-1}, $K_2 = 86.4 \pm 3.2$ km s^{-1}, $\gamma_1 = 25.9^{+2.2}_{-2.1}$ km s^{-1}, $\gamma_2 = 45.0 \pm 2.8$ km s^{-1}, $\gamma_2 - \gamma_1 = 19.1 \pm 3.5$ km s^{-1}, and $K_1/K_2 = 1.573^{+0.074}_{-0.062}$.

Fig. 3 shows the radial velocities and the Lomb–Scargle diagram for PG 1632+177. Excluding a single spectrum where both lines are blended, we have 15 velocity measurements for this system. The orbital period for this binary is relatively well constrained to about 2 d, though significant aliasing is present in the Lomb–Scargle diagram. Performing the orbital fits 1000 times based on a Monte Carlo analysis, the best-fitting orbital elements for PG 1632+177 are $P = 2.049\,87^{+0.011\,23}_{-0.005\,69}$ d, $K_1 = 78.2 \pm 2.0$ km s^{-1}, $K_2 = 58.4 \pm 1.9$ km

s^{-1}, $\gamma_1 = 16.6 \pm 1.7$ km s^{-1}, $\gamma_2 = 20.8 \pm 1.9$ km s^{-1}, $\gamma_2 - \gamma_1 = 4.1^{+2.8}_{-3.4}$ km s^{-1}, and $K_1/K_2 = 1.342^{+0.051}_{-0.056}$.

6 ATMOSPHERIC PARAMETER DETERMINATION

As mentioned in Section 2, the overluminosity of our targets manifests itself as a severe discrepancy between their spectroscopic and parallax distances. Another way to look at this is to compare the atmospheric parameters obtained from spectroscopy and photometry under the assumption of a single star. With this in mind, for each system, we fit available observed photometry with synthetic photometry computed from single white dwarf model atmospheres (see, e.g. Bergeron, Leggett & Ruiz 2001).

We use SDSS *ugriz* magnitudes for both targets (Ahumada et al. 2020), as well as Johnson *JHK* magnitudes for WD 1534+503 (Zuckerman et al. 2003) and 2MASS JHK$_s$ magnitudes for PG 1632+177 (Skrutskie et al. 2006). We also assume the *Gaia* DR2 distances (Gaia Collaboration et al. 2018). We obtain $T_{\rm eff} = 8870 \pm 260$ K, $\log g = 7.26 \pm 0.07$ for WD 1534+503, and $T_{\rm eff} = 10,090 \pm 190$ K, $\log g = 7.23 \pm 0.03$ for PG 1632+177. In both cases, compared to the spectroscopic solutions of Gianninas et al. (2011) reported in Section 2, the effective temperatures are similar while the surface gravities are significantly lower. This is typical of unresolved binary systems: a photometric analysis assuming a single star always yields a very large radius (corresponding to a very low mass white dwarf) to artificially match the high luminosity produced by the two components (see, e.g. Bédard et al. 2017).

In order to constrain the atmospheric parameters of both components in WD 1534+503 and PG 1632+177, we rely on the deconvolution procedure introduced by Bédard et al. (2017, see also Kilic et al. 2020). This method involves fitting simultaneously the observed Balmer lines and spectral energy distribution with composite model atmospheres. We use the optical spectra from Gianninas et al. (2011) that include Hβ through H8, the optical and near-infrared photometry mentioned above, and the *Gaia* DR2 parallaxes. The only change in our theoretical framework is that we use the new evolutionary sequences of Bédard et al. (2020) in place of the older calculations of Fontaine, Brassard & Bergeron (2001). Note that these sequences are appropriate for CO-core white dwarfs, while we show below that WD 1534+503 and PG 1632+177 each likely contain a low-mass He-core component. However, a comparison with the He-core sequences of Althaus, Miller Bertolami & Córsico (2013) shows that this small inconsistency has only a minor impact on our derived parameters (i.e. a change of ≈0.03 M$_\odot$ for given values of $T_{\rm eff}$ and $\log g$).

A priori, our fitting procedure involves four free parameters: $T_{\rm eff,\,1}$, $T_{\rm eff,\,2}$, $\log g_1$, and $\log g_2$. However, the individual masses of the components in a white dwarf binary can be derived from the orbital parameters. Since the difference in systemic velocities is equal to the difference in gravitational redshifts, a combination of this velocity offset ($\gamma_2 - \gamma_1$) with the mass ratio of the binary (derived from K_1/K_2) determines M_1 and M_2, and hence $\log g_1$ and $\log g_2$, given a set of evolutionary sequences. Nevertheless, this approach works well only if K_1/K_2 and ($\gamma_2 - \gamma_1$) are well constrained. For WD 1534+503, there is no significant trend in K_1/K_2 or ($\gamma_2 - \gamma_1$) with the chosen period. However, this is not true for PG 1632+177; there is a clear trend in the velocity offset based on the best-fitting period. For the top four significant aliases between 2.044 and 2.061 d, K_1/K_2 slightly changes from 1.33 to 1.36 with increasing period, but ($\gamma_2 - \gamma_1$) decreases from $5.5^{+1.8}_{-2.8}$ to $2.5^{+3.4}_{-1.7}$ km s^{-1}. Hence, the mass ratio of the binary (through K_1/K_2) is much better constrained compared to the velocity offset of the two stars. Therefore, for both systems, we rely solely on the mass ratio in our fitting procedure and use the velocity offset only as a consistency check on our best-fitting solution. This means that $T_{\rm eff,\,1}$, $T_{\rm eff,\,2}$, and $\log g_1$ are allowed to vary, while $\log g_2$ is fixed by the mass ratio.

Fig. 4 displays our best-fitting solutions. Our fitting method yields $T_{\rm eff,\,1} = 8900 \pm 500$ K, $T_{\rm eff,\,2} = 8500 \pm 500$ K, $\log g_1 = 7.60 \pm 0.15$, and $\log g_2 = 8.03^{+0.18}_{-0.16}$ for the WD 1534+503 system. Both the spectroscopic and photometric data are nicely reproduced by our composite model. The masses of the two stars are $M_1 = 0.392^{+0.069}_{-0.059}$ and $M_2 = 0.617^{+0.110}_{-0.096}$ M$_\odot$, with an estimated difference in gravitational redshifts of $16.2^{+6.3}_{-4.4}$ km s^{-1}. The latter is entirely consistent with $\gamma_2 - \gamma_1 = 19.1 \pm 3.5$ km s^{-1} estimated from the radial velocity data.

Similarly, our composite model fit reproduces the spectroscopy and photometry for the PG 1632+177 binary relatively well, with the best-fitting parameters of $T_{\rm eff,\,1} = 8800 \pm 500$ K, $T_{\rm eff,\,2} = 11,200 \pm 500$ K, $\log g_1 = 7.60 \pm 0.15$, and $\log g_2 = 7.86^{+0.17}_{-0.16}$. The masses of the two stars are $M_1 = 0.392^{+0.069}_{-0.059}$ and $M_2 = 0.526^{+0.095}_{-0.082}$ M$_\odot$, with an estimated difference in gravitational redshifts of $8.6^{+3.6}_{-2.6}$ km s^{-1}. The latter is higher than the value obtained from the orbital fits, $\gamma_2 - \gamma_1 = 4.1^{+2.8}_{-3.4}$ km s^{-1}, but the 1σ confidence intervals overlap. The orbital and physical parameters of both systems are presented in Table 1. As mentioned above, our mass estimates likely suffer from a small systematic effect due to our use of CO-core models to analyse the low-mass components. The use of more realistic He-core models would increase the masses by ≈ 0.03 M$_\odot$.

7 NLTE EFFECTS IN COOL WHITE DWARFS

As a further check on our atmospheric parameter determination, we can compare the observed double Hα feature to that predicted by our best-fitting solution, as was done by Kilic et al. (2020) for the two double-lined systems in their sample. In this comparison, Kilic et al. used the synthetic spectra of Tremblay & Bergeron (2009) assuming local thermodynamic equilibrium (LTE), which yielded a reasonably good agreement. Applying the same set of LTE model spectra to the double Hα feature of WD 1534+503 and PG 1632+177, we surprisingly obtain a much poorer agreement, the predicted line cores being too shallow. Varying the atmospheric parameters only makes the situation worse, suggesting that the problem does not lie in our deconvolution procedure, but rather in the synthetic spectra themselves. NLTE effects appear as the most plausible explanation, since these are expected to be important in the core of the Hα line (Heber, Napiwotzki & Reid 1997; Koester et al. 1998).

To investigate this idea, we compute NLTE synthetic spectra of H-atmosphere white dwarfs using the code SYNSPEC, version 51 (Hubeny & Lanz 2011, 2017). We use the LTE model atmospheres of Tremblay & Bergeron (2009) as input and perform NLTE line formation calculations keeping the atmospheric structures fixed. This is an excellent approximation for our purpose, because the core of the Hα line is formed high in the atmosphere, where the radiation field is largely decoupled from the temperature and pressure structures (Heber et al. 1997; Koester et al. 1998). In order to model the pressure-broadened Balmer lines of cool white dwarfs properly, both Stark and neutral broadening must be taken into account (Bergeron, Wesemael & Fontaine 1991). We rely on the state-of-the-art Stark profiles of Tremblay & Bergeron (2009) and on our own implementation in SYNSPEC of a detailed treatment of neutral broadening, including both resonant and non-resonant processes,

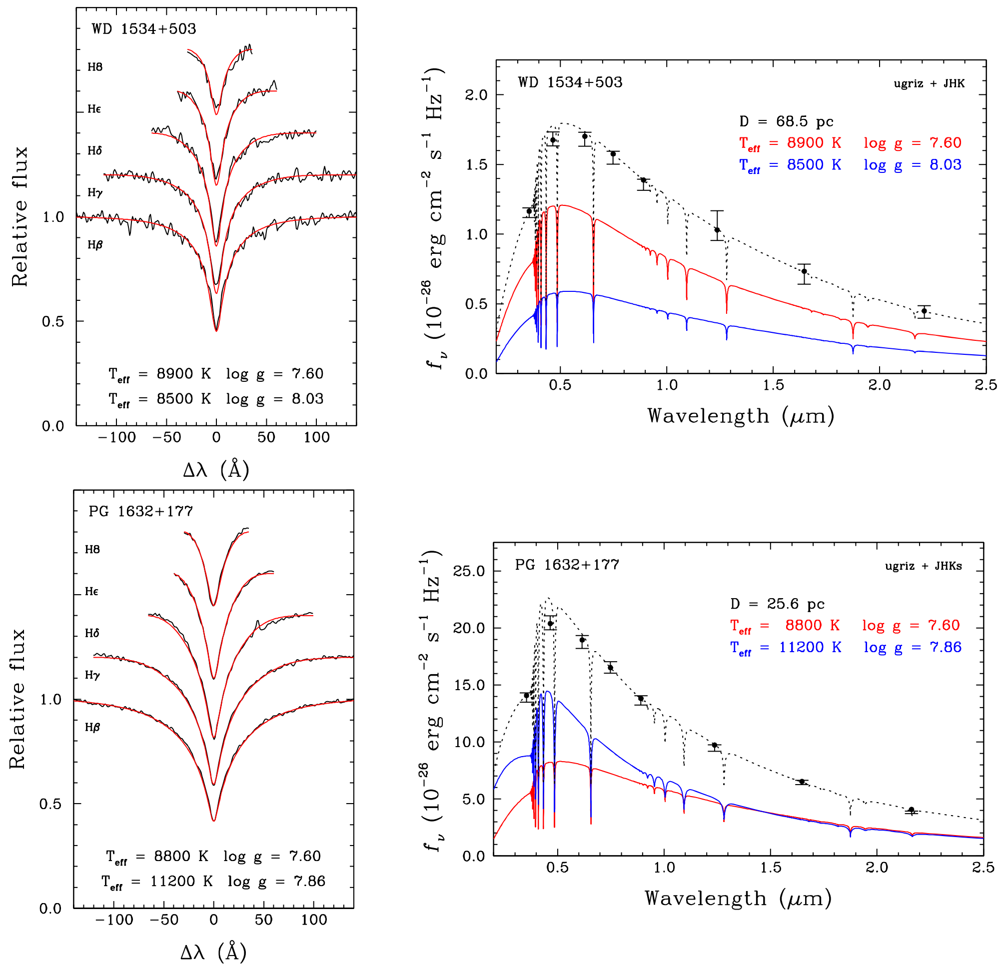

Figure 4. Best model-atmosphere fits to the Balmer lines (left-hand panels) and the spectral energy distributions (right-hand panels) of WD 1534+503 and PG 1632+177. In the left-hand panels, the observed and synthetic spectra are displayed as the black and red lines, respectively. In the right-hand panels, the observed and synthetic average fluxes are shown as the error bars and filled circles, respectively; in addition, the red and blue lines show the contribution of each component to the total monochromatic model flux, which is displayed as a black dotted line. The best-fitting atmospheric parameters are given in each panel.

Table 1. Orbital and physical parameters of the two binary systems presented in this paper.

Parameter	WD 1534+503	PG 1632+177
Period (d)	$0.711\,29^{+0.002\,86}_{-0.001\,35}$	$2.049\,87^{+0.011\,23}_{-0.005\,69}$
K_1 (km s^{-1})	$135.9^{+3.3}_{-3.1}$	78.2 ± 2.0
K_2 (km s^{-1})	86.4 ± 3.2	58.4 ± 1.9
γ_1 (km s^{-1})	$25.9^{+2.2}_{-2.1}$	16.6 ± 1.7
$\gamma_2 - \gamma_1$ (km s^{-1})	19.1 ± 3.5	$4.1^{+2.8}_{-3.4}$
K_1/K_2	$1.573^{+0.074}_{-0.062}$	$1.342^{+0.051}_{-0.056}$
$T_{\rm eff,\,1}$ (K)	8900 ± 500	8800 ± 500
$T_{\rm eff,\,2}$ (K)	8500 ± 500	11, 200 ± 500
M_1 (M$_\odot$)	$0.392^{+0.069}_{-0.059}$	$0.392^{+0.069}_{-0.059}$
M_2 (M$_\odot$)	$0.617^{+0.110}_{-0.096}$	$0.526^{+0.095}_{-0.082}$
DR2 Parallax (mas)	14.5891 ± 0.0348	39.0471 ± 0.0329
EDR3 Parallax (mas)	14.6603 ± 0.0284	39.0340 ± 0.0197

Notes. Note that masses are obtained using CO-core models. He-core models result in an increase of ≈ 0.03 M$_\odot$ for the low-mass components.

following Ali & Griem (1965), Ali & Griem (1966), and Lewis (1967). Finally, the continuum opacity of H$^-$, which is significant in cool H-atmosphere white dwarfs, is considered in our calculations as a 'background' LTE opacity. Our grid of NLTE synthetic spectra covers $T_{\rm eff}$ = 5000–20 000 K and log g = 7.0–9.0. We also generate a similar grid in LTE to allow a direct comparison with the LTE grid of Tremblay & Bergeron (2009) and thereby validate our modifications to SYNSPEC.

Fig. 5 displays our new NLTE theoretical H α line profiles at log g = 8.0 and various effective temperatures (solid curves). Also shown are the results of our corresponding LTE calculations (dashed curves) as well as those of Tremblay & Bergeron (2009, dotted curves). The agreement between both sets of LTE line profiles is excellent, giving us confidence that we have correctly included the appropriate physics in SYNSPEC. Furthermore, the NLTE treatment results in deeper line cores, as expected (Koester et al. 1998). Interestingly, the magnitude of the NLTE effects actually increases with decreasing effective temperature, contrary to what is seen in very hot white dwarfs (Napiwotzki 1997). To our knowledge, this is the first time that this behaviour of NLTE effects in cool white dwarfs is reported. This result nicely explains why LTE line profiles were sufficient to reproduce the H α observations in Kilic et al. (2020) but not in this work. Indeed, the double-lined systems analysed by Kilic et al.

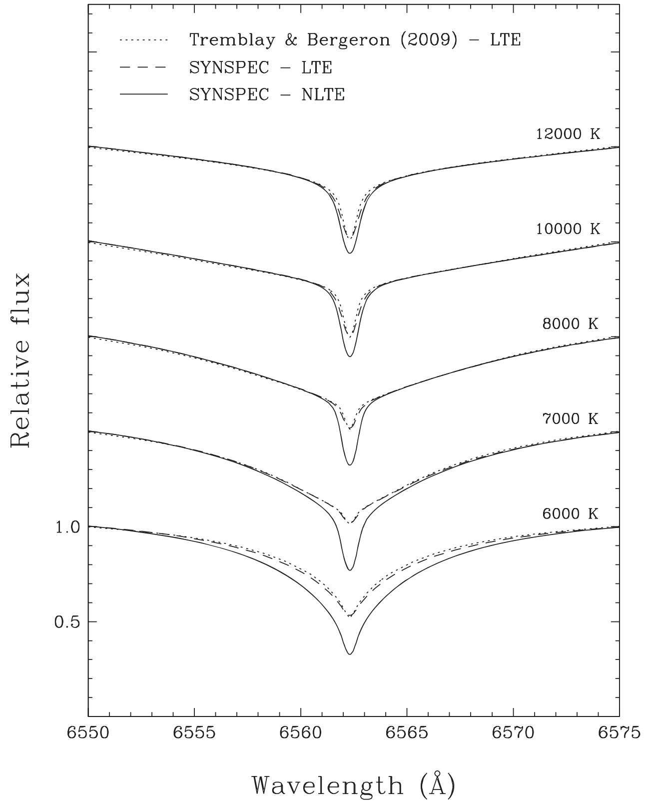

Figure 5. Comparison of theoretical H α line profiles at $\log g = 8.0$ and various effective temperatures (indicated in the figure) from three different model grids: the LTE grid of Tremblay & Bergeron (2009, dotted curves), and our own LTE (dashed curves) and NLTE (solid curves) grids computed with SYNSPEC. The synthetic spectra are normalized to a continuum set to unity and are offset vertically by 0.5 for clarity.

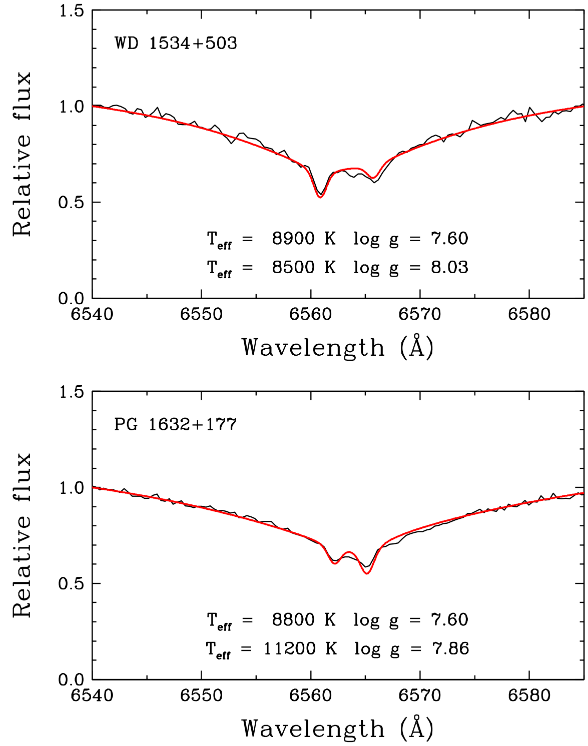

Figure 6. Comparison of the observed (black) and predicted (red) double H α features of WD 1534+503 and PG 1632+177.

contain relatively hot objects with $T_{\rm eff} \sim 12\,000$–$13\,000$ K, for which the difference between the LTE and NLTE line cores is quite small. On the other hand, WD 1534+503 and PG 1632+177 both include cooler components with $T_{\rm eff} \sim 8000$–9000 K, for which the NLTE effect is more pronounced.

Fig. 6 compares the observed double H α features of both WD 1534+503 and PG 1632+177 with those predicted by our NLTE calculations using the best-fitting atmospheric parameters. We improve the signal-to-noise ratio by co-adding several of our Gemini spectra at the same orbital phase. The predicted NLTE line cores agree reasonably well with the observed profiles, though the line core for the hotter component in PG 1632+177 is predicted slightly too deep. This comparison demonstrates the robustness of our atmospheric solutions, as we simply overplot the predicted line profiles from our model fits that do not use these data.

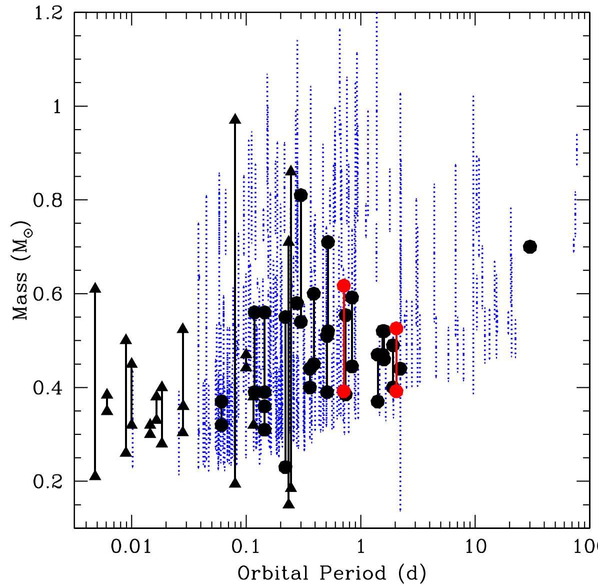

Figure 7. Mass and orbital period distribution of known SB2 (circles) and eclipsing (triangles) double white dwarfs compared to the predictions from binary population synthesis models. The lines connect the components of each observed (solid lines) and simulated (dotted lines) binary. The red symbols mark WD 1534+503 and PG 1632+177.

8 DISCUSSION

Fig. 7 shows the mass and orbital period distribution of all known double-lined spectroscopic binary (SB2) white dwarfs with orbital constraints, including WD 1534+503 and PG 1632+177, and eclipsing double white dwarfs (Burdge et al. 2020; Hallakoun et al. 2016, and references therein), along with the predictions from population synthesis models (Breivik et al. 2020). The observed population is dominated by low-mass He-core white dwarfs. For example, the two newly discovered systems presented here, WD 1534+503 and PG 1632+177, both contain low-mass white dwarfs with $M \approx 0.39\,{\rm M}_{\odot}$ and likely CO-core companions.

There are significant selection biases that favour the discovery of low-mass white dwarf systems. Since such white dwarfs are significantly larger than their more massive CO core counterparts, they are overrepresented in magnitude-limited surveys, and they are more likely to show photometric effects like eclipses and ellipsoidal variations, and are therefore easier to discover in transient surveys like the Zwicky Transient Facility (Burdge et al. 2020). The shortest period systems, with periods of tens of minutes (Brown et al. 2011; Burdge et al. 2020), were found by a highly selective search and cannot be compared to the other white dwarfs or simulations.

Many SB2 white dwarf binaries are targeted due to their overluminosity in colour–magnitude diagrams, which again favour nearby, lower mass systems. Since the detection of the double-lines typically require high-resolution spectroscopy, the SB2 systems currently known (excluding the eclipsing systems) are restricted to relatively bright white dwarfs with $G \leq 16$ mag.

To simulate the mass and orbital period distribution of short-period double white dwarfs, we use the population synthesis code COSMIC (Breivik et al. 2020) to track the evolution of 10^5 main-sequence binaries assuming a constant star formation rate and a 10-Gyr-old population. We use independently distributed parameters with primary masses following the Kroupa, Tout & Gilmore (1993) initial-mass function, a thermal eccentricity distribution, uniformly sampled mass ratios, and log-uniformly sampled orbital separations, and assume the common-envelope efficiency parameter alpha1 = 1, and the binding energy factor for common envelope evolution lambdaf = 0.5 (see Breivik et al. 2020, for details). We randomly generate a distance to each simulated binary (assuming a constant density) within 100 pc.

For a fair comparison with the observational sample, here we limit the simulated sample to He- and CO-core white dwarfs, and only show the simulated binaries brighter than 16th mag, and where both stars in the system have $T_{\rm eff} \geq 6000$ K. The selection in magnitude ensures that the fainter CO + CO white dwarf binaries are underrepresented as in the observational sample, and the selection in temperature ensures that both white dwarfs would display relatively deep H α lines, if they have H-rich atmospheres, and therefore these systems would be classified SB2. The dotted lines in the figure connect the components of each simulated binary.

Fig. 7 demonstrates that the orbital period and mass distribution of the observed SB2 and eclipsing double white dwarfs is remarkably similar to the predictions from the binary population synthesis models. The latter predict that the lower mass He-core white dwarfs are preferentially found in shorter period systems (see also Nelemans et al. 2001), which is consistent with the observed sample. The population synthesis models also predict heavier CO + CO white dwarf binaries at short (<1 d) periods, but these tend to be, on average, fainter, and therefore harder to find. Models also predict binaries with orbital periods longer than a few days. However, the observational sample is significantly biased against such systems, and currently all but one (WD1115+166; Maxted et al. 2002) of the SB2 white dwarfs known have orbital periods shorter than about 2.2 d. The identification of longer period systems is challenging (see for example Napiwotzki et al. 2020), but may be possible with large-scale astrometric or spectroscopic surveys like *Gaia* (Andrews, Breivik & Chatterjee 2019), the Dark Energy Spectroscopic Instrument (DESI) Milky Way Survey (Allende Prieto et al. 2020), or the SDSS-V (Kollmeier et al. 2019).

Fig. 8 shows a colour–magnitude diagram of the 100-pc white dwarfs from the Montreal White Dwarf Database (MWDD; Dufour et al. 2017), along with the cooling sequences for 0.2-, 0.4-, 0.6-, 0.8-, 1.0-, 1.2-, and 1.3-$M_\odot$ pure-H atmosphere white dwarfs. To create a relatively clean white dwarf sample, here we only include spectroscopically confirmed and candidate (CND) white dwarfs as defined in the MWDD, and exclude the candidates that appear only in the Gentile Fusillo et al. (2019) catalogue. The previously known SB2

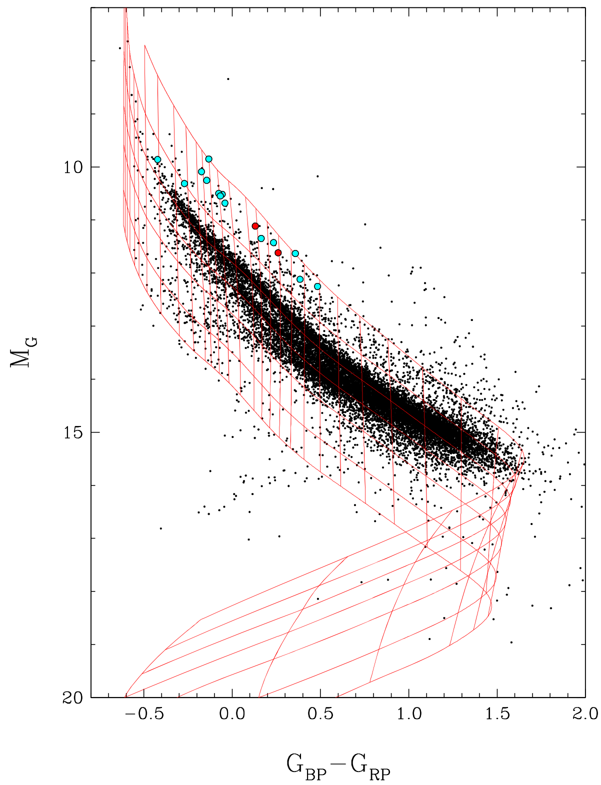

Figure 8. *Gaia* colour–magnitude diagram of the 100-pc MWDD (Dufour et al. 2017) sample. Red lines show the cooling sequences for pure-H atmosphere white dwarf models with 0.2, 0.4, 0.6, 0.8, 1.0, 1.2, and 1.3 $M_\odot$ (from the top to bottom). Cyan points mark the previously known double-lined spectroscopic binaries within 100 pc, and the red points mark WD 1534+503 and PG 1632+177.

white dwarfs and the newly identified systems (WD 1534+503 and PG 1632+177) are marked with cyan and red symbols, respectively. The current sample of SB2 white dwarfs represents only the tip of the iceberg; there are a large number of overluminous white dwarfs within 100 pc of the Sun, ∼30 per cent of which should be double-lined (Kilic et al. 2020). Follow-up observations of these overluminous white dwarfs is guaranteed to significantly enlarge the SB2 white dwarf population in the solar neighborhood (Marsh 2019).

9 CONCLUSIONS

Gaia DR2 parallaxes provide a novel method to identify double white dwarfs through their overluminosity. In addition, double-lined systems can be identified based on inconsistencies between their spectroscopic distances and parallaxes (Bédard et al. 2017). Here, we present follow-up spectroscopy of two such white dwarfs where the spectroscopic and parallax distances differ by about 50 per cent. We show that WD 1534+503 and PG 1632+177 are double-lined white dwarfs with orbital periods of 0.71 and 2.05 d, respectively.

We constrain the atmospheric parameters of both components in each system through a composite model-atmosphere analysis using a new set of NLTE synthetic spectra for cool white dwarfs. We demonstrate that the NLTE effects in the H α line core increase with decreasing effective temperature. The predicted NLTE line cores agree well with the observed H α profiles in WD 1534+503 and PG 1632+177. Both systems contain a low-mass He-core white dwarf with a likely CO-core white dwarf companion. After L 870−2, PG

1632+177 becomes the second closest double-lined white dwarf binary currently known.

We discuss the orbital period and mass distribution of the SB2 white dwarfs, and demonstrate that the observed population is consistent with the predictions from the binary population synthesis models, though the more massive, short-period CO + CO white dwarfs are still waiting to be discovered in large numbers.

ACKNOWLEDGEMENTS

We thank Ralf Napiwotzki for a constructive referee report, Jeff Andrews for useful discussions on COSMIC, and Siyi Xu for helping us actively define the cadence of our Gemini observations. This work is supported in part by the NSF under grant AST-1906379, the NSERC Canada, and by the Fund FRQ-NT (Québec).

This paper is based on observations obtained at the Gemini Observatory, which is operated by the Association of Universities for Research in Astronomy, Inc., under a cooperative agreement with the NSF on behalf of the Gemini partnership: the National Science Foundation (United States), National Research Council (Canada), CONICYT (Chile), Ministerio de Ciencia, Tecnología e Innovación Productiva (Argentina), Ministério da Ciência, Tecnologia e Inovação (Brazil), and Korea Astronomy and Space Science Institute (Republic of Korea).

This work was supported by a NASA Keck PI Data Award, administered by the NASA Exoplanet Science Institute. Data presented herein were obtained at the W. M. Keck Observatory from telescope time allocated to the National Aeronautics and Space Administration through the agency's scientific partnership with the California Institute of Technology and the University of California. The Observatory was made possible by the generous financial support of the W. M. Keck Foundation.

DATA AVAILABILITY

The data underlying this paper are available in the Gemini Observatory Archive at https://archive.gemini.edu/ and the Keck Observatory Archive at https://koa.ipac.caltech.edu/cgi-bin/KOA/nph-KOAlogin, and can be accessed with the program numbers GN-2020A-Q-221 and N018 (or UT 20180618) for Gemini and Keck, respectively.

REFERENCES

Ahumada R. et al., 2020, ApJS, 249, 3
Ali A., Griem H., 1965, Phys. Rev., 140, A1044
Ali A., Griem H., 1966, Phys. Rev., 144, 366
Allende Prieto C. et al., 2020, Res. Notes AAS, 4, 188
Althaus L. G., Miller Bertolami M. M., Córsico A. H., 2013, A&A, 557, A19
Andrews J. J., Breivik K., Chatterjee S., 2019, ApJ, 886, 68
Bédard A., Bergeron P., Fontaine G., 2017, ApJ, 848, 11
Bédard A., Bergeron P., Brassard P., Fontaine G., 2020, ApJ, 901, 93
Bergeron P., Wesemael F., Fontaine G., 1991, ApJ, 367, 253
Bergeron P., Leggett S. K., Ruiz M. T., 2001, ApJS, 133, 413
Breivik K. et al., 2020, ApJ, 898, 71
Brown W. R., Kilic M., Allende Prieto C., Kenyon S. J., 2010, ApJ, 723, 1072
Brown W. R., Kilic M., Hermes J. J., Allende Prieto C., Kenyon S. J., Winget D. E., 2011, ApJ, 737, L23
Brown W. R. et al., 2020, ApJ, 889, 49
Burdge K. B. et al., 2019a, Nature, 571, 528
Burdge K. B. et al., 2019b, ApJ, 886, L12
Burdge K. B. et al., 2020, ApJ, 905, 26
De Lee N. et al., 2013, AJ, 145, 155
Dufour P., Blouin S., Coutu S., Fortin-Archambault M., Thibeault C., Bergeron P., Fontaine G., 2017, in Tremblay P. E., Gaensicke B., Marsh T., eds, ASP Conf. Ser. Vol. 509, 20th European White Dwarf Workshop. Astron. Soc. Pac., San Francisco, p. 3
Fontaine G., Brassard P., Bergeron P., 2001, PASP, 113, 409
Gaia Collaboration et al., 2018, A&A, 616, A10
Gentile Fusillo N. P. et al., 2019, MNRAS, 482, 4570
Gianninas A., Bergeron P., Ruiz M. T., 2011, ApJ, 743, 138
Hallakoun N. et al., 2016, MNRAS, 458, 845
Heber U., Napiwotzki R., Reid I. N., 1997, A&A, 323, 819
Hollands M. A., Tremblay P. E., Gänsicke B. T., Gentile-Fusillo N. P., Toonen S., 2018, MNRAS, 480, 3942
Hubeny I., Lanz T., 2011, Astrophysics Source Code Library, record ascl:1109.022
Hubeny I., Lanz T., 2017, preprint (arXiv:1706.01859)
Kilic M., Brown W. R., Allende Prieto C., Kenyon S. J., Panei J. A., 2010, ApJ, 716, 122
Kilic M., Bédard A., Bergeron P., Kosakowski A., 2020, MNRAS, 493, 2805
Kleinman S. J. et al., 2013, ApJS, 204, 5
Koester D., Dreizler S., Weidemann V., Allard N. F., 1998, A&A, 338, 612
Kollmeier J. et al., 2019, BAAS, 51, 274
Korol V., Rossi E. M., Groot P. J., Nelemans G., Toonen S., Brown A. G. A., 2017, MNRAS, 470, 1894
Kroupa P., Tout C. A., Gilmore G., 1993, MNRAS, 262, 545
Lewis E., 1967, Proc. Phys. Soc., 92, 817
Marsh T., 2019, The Beginnings and Ends of Double White Dwarfs, Available at: https://doi.org/10.5281/zenodo.3265937
Marsh T. R., Dhillon V. S., Duck S. R., 1995, MNRAS, 275, 828
Maxted P. F. L., Burleigh M. R., Marsh T. R., Bannister N. P., 2002, MNRAS, 334, 833
Napiwotzki R., 1997, A&A, 322, 256
Napiwotzki R. et al., 2020, A&A, 638, A131
Nelemans G., Yungelson L. R., Portegies Zwart S. F., Verbunt F., 2001, A&A, 365, 491
Newville M., Stensitzki T., Allen D. B., Ingargiola A., 2014, LMFIT: Non-Linear Least-Square Minimization and Curve-Fitting for Python, Available at: http://doi.org/10.5281/zenodo.11813
Nissanke S., Vallisneri M., Nelemans G., Prince T. A., 2012, ApJ, 758, 131
Rebassa-Mansergas A., Toonen S., Korol V., Torres S., 2019, MNRAS, 482, 3656
Saffer R. A., Liebert J., Olszewski E. W., 1988, ApJ, 334, 947
Saffer R. A., Livio M., Yungelson L. R., 1998, ApJ, 502, 394
Skrutskie M. F. et al., 2006, AJ, 131, 1163
Tremblay P. E., Bergeron P., 2009, ApJ, 696, 1755
Tremblay P. E., Bergeron P., Gianninas A., 2011, ApJ, 730, 128
Tremblay P. E., Ludwig H. G., Steffen M., Freytag B., 2013, A&A, 559, A104
Vogt S. S. et al., 1994, in Crawford D. L., Craine E. R., eds, Proc. SPIE Conf. Ser. Vol. 2198, Instrumentation in Astronomy VIII. SPIE, Bellingham, p. 362
Zuckerman B., Koester D., Reid I. N., Hünsch M., 2003, ApJ, 596, 477

APPENDIX A: RADIAL VELOCITY DATA

Table A1. Radial velocities for WD 1534+503.

HJD−2458000 (days)	$V1_{helio}$ (km s^{-1})	$V2_{helio}$ (km s^{-1})
287.80826950	−79.8 ± 2.4	95.0 ± 13.7
1033.75755063	125.2 ± 7.5	−21.2 ± 12.4
1033.88721649	−14.0 ± 15.7	57.6 ± 24.0
1033.99645563	−103.8 ± 7.0	130.5 ± 10.3
1034.76117037	−112.8 ± 5.9	132.0 ± 11.0
1034.84874668	−43.8 ± 4.0	95.1 ± 3.8
1034.93651786	44.3 ± 3.7	44.3 ± 3.7
1037.81231324	95.0 ± 15.6	17.2 ± 30.1
1037.97750948	151.5 ± 5.4	−36.0 ± 4.9
1038.77259600	76.1 ± 7.8	−10.4 ± 23.1
1038.93972014	−95.9 ± 8.2	115.6 ± 10.9
1039.75191944	−90.9 ± 10.6	98.0 ± 20.0
1039.75559118	−92.3 ± 8.0	121.3 ± 5.9
1039.89359319	45.3 ± 3.3	45.3 ± 3.3
1039.97106002	115.6 ± 6.9	−12.2 ± 17.4

Table A2. Radial velocities for PG 1632+177.

HJD−2458000 (days)	$V1_{helio}$ (km s^{-1})	$V2_{helio}$ (km s^{-1})
287.74574073	85.6 ± 1.8	−27.7 ± 2.2
287.74978969	86.8 ± 1.7	−30.0 ± 1.9
287.79859253	87.9 ± 1.3	−33.9 ± 1.2
287.84337570	93.0 ± 1.2	−36.4 ± 1.2
1030.76643626	−52.5 ± 6.6	64.0 ± 5.0
1030.93104515	−63.6 ± 4.8	79.1 ± 5.7
1031.76860075	81.5 ± 6.9	−31.4 ± 7.1
1031.88742845	88.8 ± 9.8	−37.4 ± 7.1
1031.99468554	97.3 ± 7.4	−34.8 ± 7.3
1033.77338563	68.8 ± 7.1	−22.7 ± 10.3
1033.91624887	90.2 ± 7.7	−38.3 ± 7.2
1034.01369802	95.9 ± 6.5	−35.8 ± 5.1
1034.95654558	−54.3 ± 5.7	83.9 ± 8.8
1037.90993764	69.1 ± 7.8	−22.5 ± 8.3
1038.92735578	−31.9 ± 8.7	92.2 ± 15.9
1039.93019040	64.8 ± 11.8	15.0 ± 39.5

This paper has been typeset from a TEX/LATEX file prepared by the author.